Molecular architecture and assembly of the yeast kinetochore MIND complex

Daniel P. Maskell, Xiao-Wen Hu, and Martin R. Singleton

Macromolecular Structure and Function Laboratory, Cancer Research UK London Research Institute, London WC2A 3PX, England, UK

The MIND multiprotein complex is a conserved, essential component of eukaryotic kinetochores and is a constituent of the tripartite KMN network that directly attaches the kinetochore to the mitotic spindle. The primary microtubule-binding complex in this network, NDC80, has been extensively characterized, but very little is known about the structure or function of the MIND complex. In this study, we present biochemical, hydrodynamic, electron microscopy, and small-angle x-ray scattering data that provide insight into the overall architecture and assembly of the MIND complex and the physical relationship of the complex with other components of the KMN network. We propose a model for the overall structure of the complex and provide data on the interactions with NDC80, Spc105p, and thus the mitotic spindle.

Introduction

The accurate segregation of sister chromatids to daughter cells during mitosis is a complex and tightly regulated process mediated by the molecular machinery of the mitotic spindle. A central component in these processes is the kinetochores, which are large proteinaceous complexes that assemble on centromeric chromatin and make attachments to the mitotic spindle (Santaguida and Musacchio, 2009). As well as providing mechanical attachment, the kinetochores are the source of the spindle assembly checkpoint, which prevents premature anaphase onset and serves to correct aberrant spindle attachments (Musacchio and Salmon, 2007). Such a complex cellular machine has many constituent parts, and an ever-increasing number of proteins have been implicated in kinetochore function. Relatively little is known about the three-dimensional structures of many of these, partly because many of the proteins form large, flexible, elongated complexes, making analysis by techniques such as x-ray crystallography problematic. In addition, kinetochore proteins seem to evolve at an unusually high rate, with wide sequence divergence between orthologues. This, together with the fact that few kinetochore proteins possess obvious enzymatic activity means that sequence-based predictions of structure and function are of limited value. Despite the overall complexity of the kinetochore, it has become apparent that there is a relatively simple, well-defined set of core protein complexes that are entirely conserved throughout evolution and are necessary for formation of a functional kinetochore (Meraldi et al., 2006). Central to these is the so-called KMN network, which itself is comprised of three subcomplexes, Knl1–Blinkin–Spc105p, MIND–Mis12–Mtw1, and NDC80 (Cheeseman et al., 2006). For clarity, we shall refer to the complexes as Knl1, MIND, and NDC80 in this paper.

The MIND complex is essential for kinetochore assembly and correct mitotic progression. Originally identified in budding yeast (Euskirchen, 2002), the complex consists of four subunits: Mtw1p (Mis12 in fission yeast and humans), Dsn1p, Nsl1p, and Nnf1p. Deletions of the MIND proteins in budding yeast are inviable (Shan et al., 1997; Goshima et al., 1999; Euskirchen, 2002), whereas temperature-sensitive mutants of both the budding and fission yeast proteins revealed a role in spindle assembly, biorientation, and chromatid segregation (Goshima and Yanagida, 2000; Scharfenberger et al., 2003). RNAi depletion of any of the constituent proteins in human (Kline et al., 2006; McAinsh et al., 2006), worm (Cheeseman et al., 2004), or fly (Przewloka et al., 2007) results in similar defects, showing delayed mitotic onset, with characteristic defects in chromosome congression, biorientation, and spindle assembly. Correct recruitment of the MIND complex is dependent on the presence of inner kinetochore proteins such as the centromeric nucleosome,

Correspondence to Martin R. Singleton: Martin.Singleton@cancer.org.uk

Abbreviations used in this paper: AUC, analytical ultracentrifugation; ITC, isothermal titration calorimetry; MBP, maltose-binding protein; MT, microtubule; SAXS, small-angle x-ray scattering; TEV, tobacco etch virus.

The Rockefeller University Press $30.00
J. Cell Biol. Vol. 190 No. 5 823–834
www.jcb.org/cgi/doi/10.1083/jcb.201002059

CENP-A^{Cse4}, and the CBF3 complex in budding yeast (Goshima et al., 1999; Scharfenberger et al., 2003). Depletion of MIND components strongly inhibits recruitment of several outer kinetochore proteins, including Ndc80 and the DAM–DASH complex (Scharfenberger et al., 2003; Kline et al., 2006), and may also affect the localization of some inner centromere proteins such as CENP-A, although there are conflicting data on this dependence. These mutational and in vivo analyses support a model in which the MIND complex is functionally downstream and physically poleward of the inner kinetochore proteins and is required for correct localization of the outer microtubule (MT)-binding proteins, as well as some checkpoint components such as Bub1, BubR1, Mad1, and Mad2 (Kline et al., 2006; McAinsh et al., 2006). The mutational phenotypes may be explained by improper establishment of kinetochore–MT attachments, coupled to perturbed activation of the spindle checkpoint.

This genetic model is supported by biochemical experiments that have demonstrated that the KMN complex is the key MT-binding site within the kinetochore (Fig. 1 a). Structural (Wei et al., 2007; Ciferri et al., 2008) and biochemical (DeLuca et al., 2005; Cheeseman et al., 2006) data have shown that the NDC80 complex can directly bind to MTs via globular heads in the Ndc80p/Nuf2p proteins that comprise a calponin homology domain. It has further been shown that the affinity of MT binding is synergistically enhanced by the presence of the other components of the KMN complex. Of these, only Knl1–Blinkin appears to have an intrinsic MT-binding activity (Cheeseman et al., 2006) in the N terminus of the protein. The exact functions of the MIND complex remain unclear. High-resolution light microscopy studies have delineated the relative positions of the main kinetochore complexes (Joglekar et al., 2006; Wan et al., 2009) and show that MIND occupies a position overlapping the inner end of NDC80 and extending toward the inner kinetochore proteins. One possibility is that MIND is a scaffold complex that links and orients the Knl1 and NDC80 complexes to allow them to contact the MT ends. Additionally, it seems probable that the MIND complex mediates the connection between the NDC80/Knl1 proteins and other, currently unidentified proteins in the inner kinetochore. In this sense, MIND is the bridge between the MT receptor complex and the inner kinetochore. The dependence on MIND of checkpoint protein recruitment suggests that it may be involved in some aspect of mitotic checkpoint activation, but whether it is directly involved in signal generation, or indirectly, as part of the MT attachment machinery is unclear. In this study, we describe the low-resolution architecture of the budding yeast MIND complex and how the constituent proteins contribute to this architecture. We also define more precisely how the MIND complex attaches to the larger KMN network.

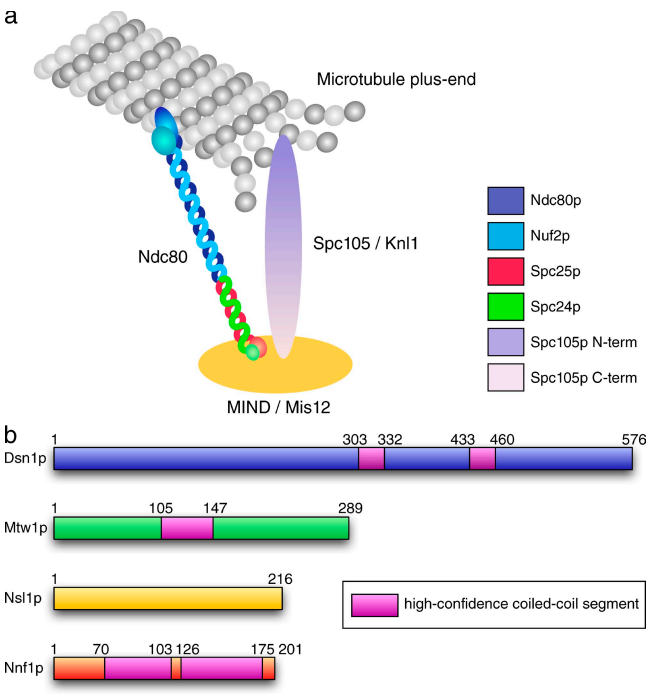

Figure 1. **Overview summary of the KMN network and MIND complex.** (a) Schematic diagram of the KMN network and proposed MT-binding model. (b) Constituent proteins of the *S. cerevisiae* MIND complex and primary structure representations. The pink sections indicate high-scoring predicted coiled-coil heptad repeats, and the numbers indicate the positions of the domain boundaries.

Results

Preparation and stoichiometry of the recombinant MIND complex

The MIND complex was prepared by coexpression in *Escherichia coli* of the four previously identified *Saccharomyces cerevisiae* constituent proteins Dsn1p, Mtw1p, Nnf1p, and Nsl1p (Euskirchen, 2002). During purification, we noticed partial dissociation of the complex into Dsn1p–Nsl1p and Mtw1p–Nnf1p heterodimers. We were able to separately express these heterodimers and reconstitute the intact complex from them, demonstrating that the tetrameric MIND complex is formed by association of tight Dsn1p–Nsl1p and Mtw1p–Nnf1p dimers (Fig. 2). These pairwise interactions are consistent with a previous yeast two-hybrid study with the human Mis12 complex (Kiyomitsu et al., 2007). Assuming one copy of each protein in the intact complex, MIND would have a calculated molecular mass of 147.9 kD. Previous experiments (De Wulf et al., 2003) have suggested that the complex may adopt differing compositions in vivo, with Flag-tagged Mtw1p identified in species of ~215, 153, and 89 kD. We do not see any evidence for these complexes with our in vitro purifications, so it is possible that the 215-kD species represents the association of MIND with another unidentified protein. The recombinant complex produced by coexpression of all four subunits in bacteria appears as a single species on a gel filtration column. The gel filtration profile of the complex has an anomalously low elution volume, suggesting that the complex may contain multiple copies of the core tetramer or adopt a highly extended conformation. To test these possibilities, we performed analytical ultracentrifugation (AUC) experiments on the recombinant protein. Sedimentation velocity experiments were initially performed to determine the molecular shape and sedimentation coefficients presented in Table I. The data show that the complex is highly elongated, with a very high axial ratio and frictional coefficient and give a derived molecular mass of 149.7 kD. Sedimentation equilibrium

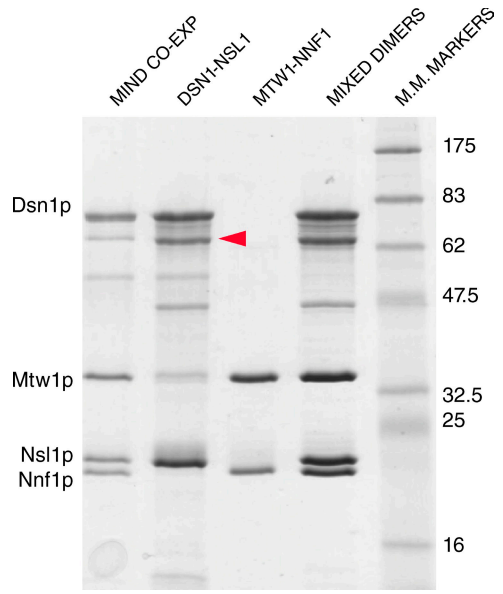

Figure 2. **SDS gel showing coexpression of the recombinant MIND subunits after purification and separate expression of the two constituent dimers.** The first lane shows intact complex from coexpression, the second lane shows the Dsn1p–Nsl1p dimer, the third lane shows the Mtw1p–Nnf1p dimer, the fourth lane shows complex reconstituted from dimers, and the fifth lane shows molecular mass (MM) markers (in kilodaltons). Note that there is some contamination of the Dsn1p–Nsl1p dimer by Hsp70 (indicated by the red arrowhead).

experiments (unpublished data) provide a consistent molecular mass and show that there is no significant self-association of the complex. Therefore, we conclude that the MIND complex is a tetramer of Dsn1p, Mtw1p, Nsl1p, and Nnf1p in a 1:1:1:1 molar ratio. We have also analyzed the hydrodynamic parameters of the constituent Dsn1p–Nsl1p and Mtw1p–Nnf1p dimers. Velocity sedimentation experiments gave molecular masses for the dimers in good agreement with calculated values (Table I). Moreover, the derived shape parameters suggest that the Mtw1p–Nnf1p dimer is the more elongated of the two species, whereas the Dsn1p–Nsl1p dimer is more compact.

EM analysis of MIND

Despite extensive efforts, we were unable to crystallize the intact MIND complex, which is unsurprising given the predicted elongated structure. Instead, we analyzed the complex using EM. Although the MIND complex is rather small for single-particle EM study, we reasoned that the extended shape might make it suitable for useful analysis.

Recombinant protein complexes were purified to homogeneity and analyzed using negative-stain EM. The complex is 21 ± 2 nm in length and has a pronounced comma shape with a globular head ~8-nm diameter and a tail of 13 ± 3 nm with a slightly globular tip (Fig. 3 a). We also examined the particles by low-angle rotary shadowing with platinum (Fig. 3 b), which showed a similar morphology to the negative-stain images, with a prominent bilobal head domain and short tail, and similar overall dimensions to the negative-stain images. The particles are homogenous at the level of overall organization; however, there does seem to be considerable conformational variability,

Table I. **Hydrodynamic parameters for intact MIND complex and constituent dimers as determined by AUC**

Sample	$S_{20,w}$	Mass	f/f_0	Stokes radius
	S	*kD*		*nm*
MIND	3.2	149.7	3.13	11.2
Dsn1/Nsl1	3.7	82.5	1.78	5.1
Mtw1/Nnf1	2.3	58.9	2.33	5.7

$S_{20,w}$ is the sedimentation coefficient normalized to water at 20°C. f/f_0 is the frictional ratio.

particularly in the head–tail angle and finer structure of the head domain. Given this variability and limited resolution of the data, it is difficult to ascribe the observed shape to specific orientations on the grids or multiple conformations of the particles. However, by selecting the most typical view, we were able to carry out two-dimensional single-particle averaging. Representative class averages are shown in Fig. 3 c. These highlight the overall arrangement of the molecule, in particular the hooklike shape of the globular head. Although the averaging probably obscures subtle differences in the conformation of the tail, the averaged images do emphasize the bulbous tip of the tail, suggesting that there is a small second globular domain present here. The thickness of the tail in the images suggests that it is unlikely to be a single coiled-coil pair as seen in the NDC80 complex (Ciferri et al., 2008), despite the fact that there are several predicted coiled-coil segments in the proteins. This is particularly apparent by direct comparison of images of MIND and NDC80; the stalk section of NDC80 is barely visible (Fig. 4 e), whereas the tail of the MIND complex is quite apparent in every particle image.

Structural studies on the NDC80 complex have shown that the conserved coiled-coil domains form an extended structure of ~55 nm (Ciferri et al., 2005; Wei et al., 2005). Sequence analysis of the NDC80 proteins together with EM images and limited proteolysis experiments allowed a model for the assembly of the complex to be proposed (Wei et al., 2005), which has since been shown to be largely correct (Ciferri et al., 2008). It is harder to make a similar analysis of the MIND complex. The predicted coiled-coil sections in the constituents of the MIND complex are shorter than those seen in the NDC80 complex and rather less well conserved, both in length and relative position, and unlike NDC80 are not at the termini of the proteins. This makes it difficult to dissect out the relative contributions of the structural domains to the formation of the complex and the overall shape.

To define the location of the individual proteins in the intact complex, we prepared a series of constructs containing the 43.4-kD maltose-binding protein (MBP) fused to the N and C termini of each of the constituent proteins. We then examined the fusion complexes by EM to locate extra density arising from the MBP fusions. Seven of the eight permutations of the complex were successfully expressed (the C-terminally tagged Mtw1p complex was unstable), although yields were extremely low and purification difficult. Despite this, we were able to obtain images of all four N-terminal fusions that consistently showed clear extra density (Fig. 3 d). In all cases, the additional density was observed in the head domain of the complex in

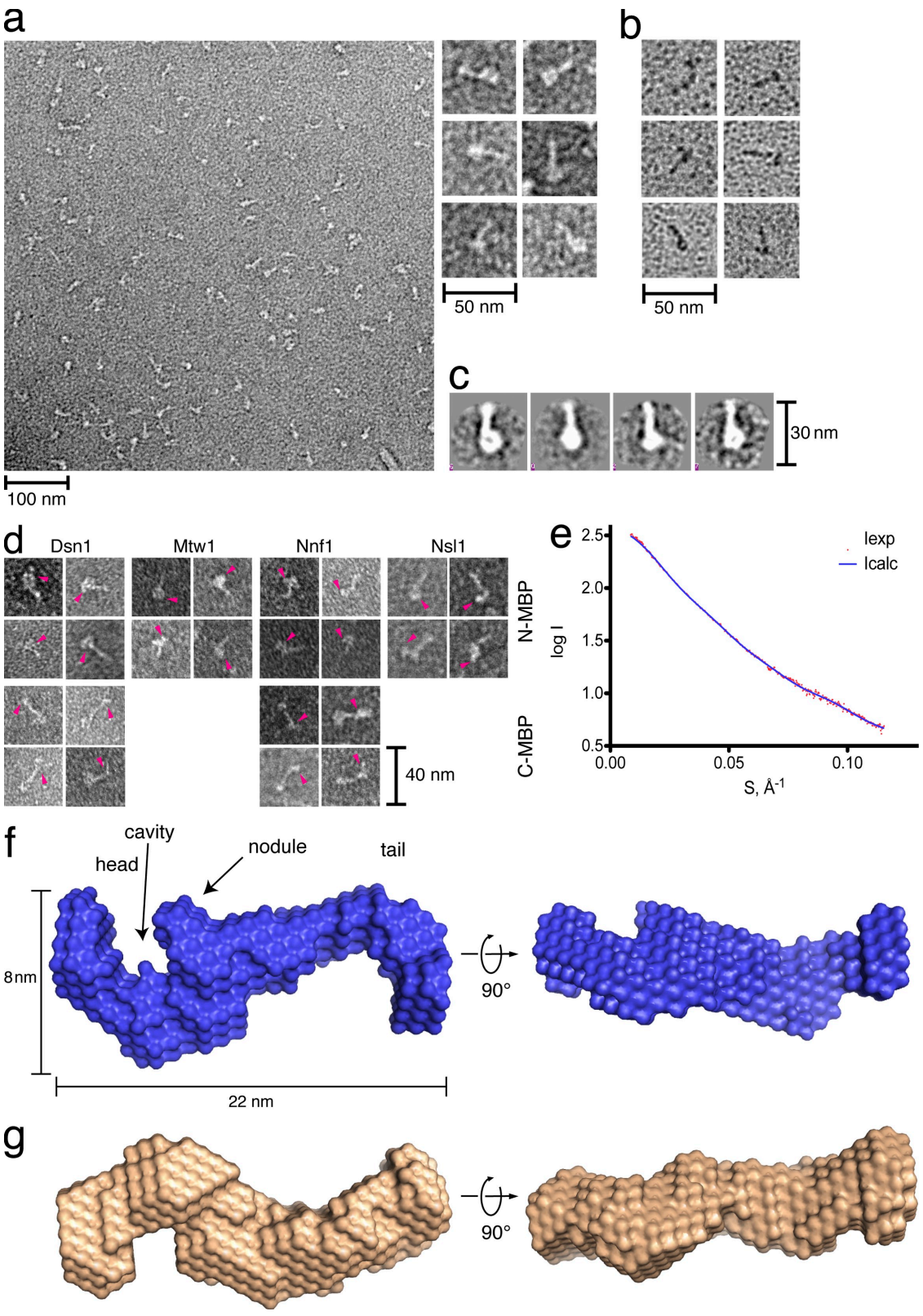

Figure 3. **Overall structure of the MIND complex as determined by EM and SAXS.** (a) EM field of negatively stained MIND complex, with individual particles shown in the adjacent panel. (b) MIND particles visualized by low-angle rotary shadowing with platinum. (c) Two-dimensional class averages of the MIND particles (n = 251). (d) EM images of N- and C-terminal MBP-MIND fusion constructs. Additional density arising from the MBP protein is indicated with pink arrowheads. (e) SAXS scattering curve (red dots) of the MIND complex, with calculated model scattering curve (blue line). Iexp, experimental scattering intensity; Icalc, calculated scattering intensity. (f) SAXS bead model reconstruction of the MIND complex. The structure shown represents results from a typical simulation. The various structural features referred to throughout the text are indicated on the model. (g) Averaged, filtered SAXS envelope derived from 30 separate ab initio reconstructions.

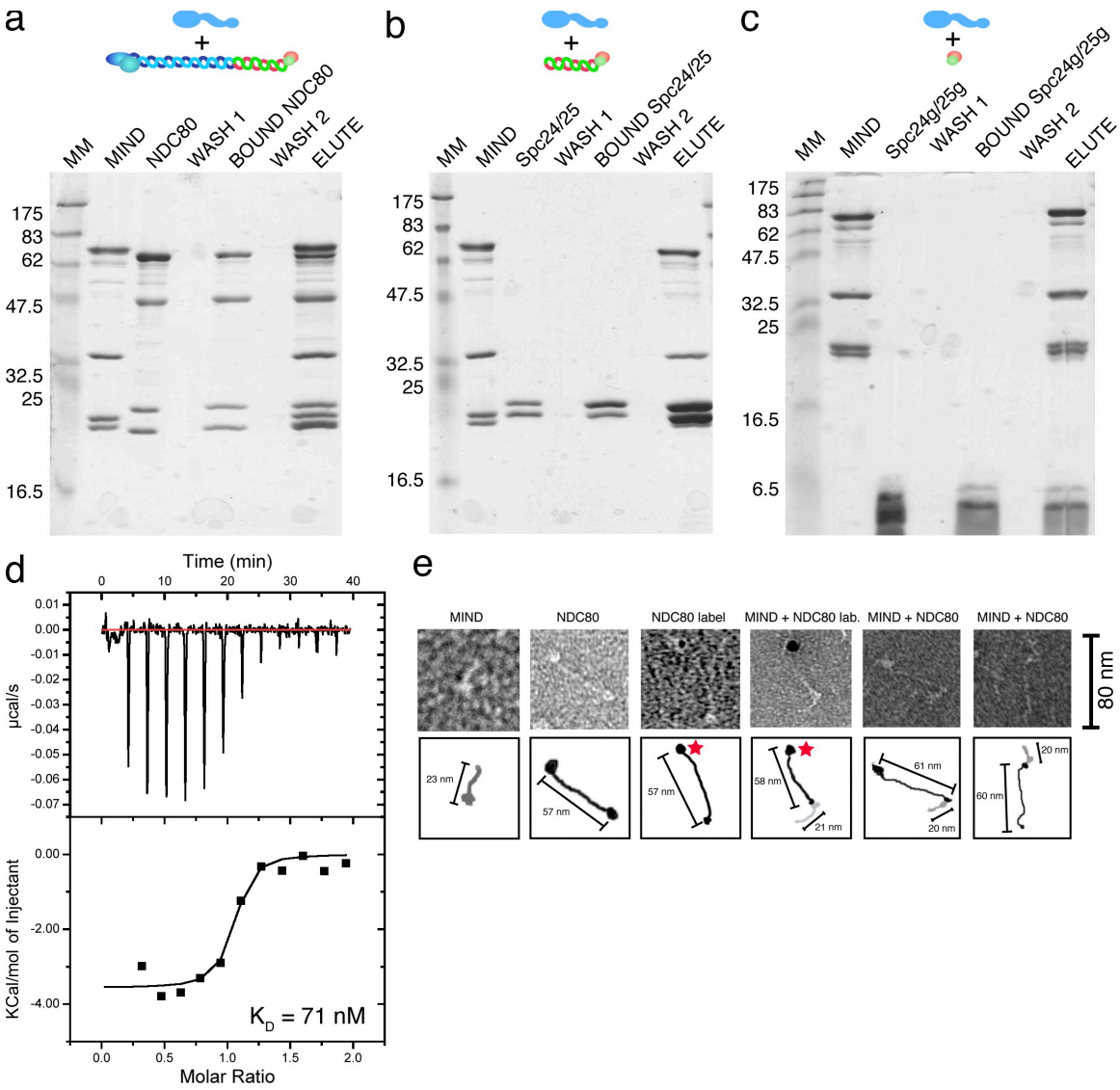

Figure 4. **SDS gels showing associations between MIND and NDC80.** (a) His-tagged NDC80 was bound to resin beads, and any excess complex was washed off. Recombinant MIND protein was then added, and the beads were again washed. The intact cocomplex was then eluted from the beads. (b and c) The same experiment was performed using Spc24p–Spc25p alone (b) and the globular domains (Spc24p$^{154–213}$–Spc25p$^{133–221}$) alone (c). (d) ITC raw data and derived binding curve for the interaction between MIND and NDC80. The red line is a normalized baseline for the experiment. (e) Single-particle EM images of the NDC80 and MIND proteins and the putative MIND–NDC80 complex. NDC80 is labeled with a gold particle at the N terminus of the Ndc80p protein. Schematic pictures are shown in the boxes below the micrographs, with NDC80 in black, MIND in gray, and the label indicated by a red star.

varying orientations, and in no case was any extra density seen in the tail domain. Equivalent experiments with N-terminal GST fusions show GST-induced dimerization via the head domain (Fig. S1 a). This strongly suggests that all four proteins in the complex partially contribute to forming the head structure. The C-terminal fusions were more heterogeneous, probably caused by the formation of complexes containing truncated fusions. The most straightforward images to interpret were those of the Nnf1p C-MBP fusion. This shows a characteristic dumbbell shape, with additional density clearly located at the end of the tail spike. The AUC data show that the Mtw1p–Nnf1p dimer is the most elongated constituent of the complex, which would be consistent with Nnf1p comprising a substantial proportion of the elongated tail structure. We also note that Nnf1p is predicted to be almost entirely coiled-coil in character and that super-resolution light microscopy data (Wan et al., 2009) indicate it to be the protein most distal to Dsn1p in vivo. Therefore, we suggest that Nnf1p forms an extended structure with the N terminus in the head and C terminus in the tail of the complex. The Nsl1p C-MBP fusions formed stable complexes, but we could see no consistent, unambiguous images that would allow us to locate the additional MBP density. Nsl1p is small and not predicted to form an extended structure. As the N terminus of the protein is clearly located in the head domain, we propose that the majority of the protein is mainly located in the head and head–tail junction region. The Dsn1p C-terminal fusions were harder to interpret, with some images showing extra density at the tail spike, although there was considerable variation in the particles and high background. As Dsn1p is the largest protein in the complex, with predicted coiled-coil character in the C terminus, we

tentatively suggest that the protein also extends the full length of the complex, with the N terminus in the head and C terminus forming part of the tail structure, as seen with Nnf1p.

Small-angle x-ray scattering (SAXS)

To validate our EM images and gain additional insights into the structure of the complex, we performed SAXS experiments on the intact complex and used ab initio modeling to generate a low-resolution structure of the complex. The distance distribution function derived from the experimental data was consistent with an elongated particle with a substantial fraction of the total particle mass at each end (Fig. S1 b). A model was generated using dummy atom–type Monte Carlo simulations that fitted the experimental data well (Fig. 3 e). A typical structure is shown in Fig. 3 f and shows the overall morphology of the particle to be similar to the EM images. The reconstruction was 23 nm long and 8 nm across the widest part of the head domain. We performed a large number of independent reconstructions against the data to assess model quality and observed some variation in the models generated (Fig. S1 c). This may arise from multiple conformations of the particle or simply reflect indeterminacy in the reconstruction procedure. However, an averaged, filtered model built from 30 separate reconstructions recapitulated the main features of the individual reconstructions (Fig. 3 g), giving us confidence in the model. The tail section of the molecule appears to be somewhat thicker than suggested by the EM images but shows the same bulbous tip. There was also a nodule on the tail section about halfway along the length of the complex in most of the reconstructions, indicating that a large folded domain of one of the head proteins resides here. Interestingly, the head of the molecule contains a large central cavity, appearing either as a hole or more frequently as a large channel, giving the head a hook shape in projection, as also seen in the EM class averages.

Formation of the KMN network and structure of the MIND–NDC80 dimer

An extensive study on the *Caenorhabditis elegans* KMN complex provided insights into the roles of the individual subcomplexes and showed how they might be combined to form a dynamic MT-binding interface (Cheeseman et al., 2006). We decided to see whether this network was conserved in *S. cerevisiae* and examined the MIND–NDC80 interaction in more detail, both biochemically and by direct visualization with EM. We first analyzed binding between the intact, full-length complexes and the constituent subcomplexes by pull-down assays. First, we demonstrated that the intact full-length complexes could bind and form a stable species containing all eight proteins (Fig. 4 a). We then showed that the Spc24p–Spc25p dimer alone is necessary and sufficient for the interaction (Fig. 4 b) and that the interaction is mediated through the globular C-terminal domains of the proteins (Spc24p residues 136–213 and Spc25p residues 116–221; Fig. 4 c). We obtained more quantitative data on the MIND–NDC80 interaction using isothermal titration calorimetry (ITC). The data are shown in Fig. 4 d and allow us to derive a K_d of 71 nM for the interaction between the full-length MIND and NDC80 complexes with 1:1 stoichiometry. We examined the full-length MIND–NDC80 interaction by EM to see whether we could directly visualize the binary complex. To differentiate the ends of the NDC80 complex, we labeled the MT-binding tip by attaching a gold bead to the N terminus of the Ndc80p protein (Fig. 4 e). We saw several NDC80 images that showed the MIND complex bound at the Spc24p–Spc25p end. The measured lengths of NDC80 and MIND in these images were consistent with those of the individual complexes. Interestingly, the complexes were not colinear; MIND always appeared angled with respect to the long axis of NDC80, although this may not be the geometry in the intact kinetochore. It appears that the interaction is between the head of the MIND complex and the Spc24p–Spc25p globular domains of NDC80. This would place the presumed Nnf1p tail furthest away from NDC80, as previously suggested (Joglekar et al., 2009; Wan et al., 2009), and suggests that this domain attaches MIND to the inner kinetochore proteins.

Interactions with Spc105p

The third member of the KMN network, Knl1, is a large protein that appears to bind MTs and directly recruits Bub1/BubR1 to the kinetochore via interactions involving tetratricopeptide repeats (Cheeseman et al., 2006; Kiyomitsu et al., 2007). The budding yeast orthologue of Knl1, Spc105p, is a 917-residue protein, which, although sharing similar overall structural organization to Knl1, is poorly conserved at a sequence level. Despite extensive efforts, we were unable to purify either full-length recombinant Spc105 or various truncated constructs. Therefore, we analyzed the interaction between MIND and Spc105 using a peptide array screen. A membrane was spotted with 21-residue peptides covering the entire Spc105 sequence with a 2-residue start increment per spot. The array was probed with full-length recombinant MIND, and bound complex was detected using antibodies against tagged Dsn1. After controlling for background, we identified two main sites of interaction, both in the C terminus of Spc105 (Fig. 5 a). This is consistent with a previous study on the human proteins, which also demonstrate an interaction between the Mis12 complex and the C terminus of Knl1 (Kiyomitsu et al., 2007). The peptides identified both constitute relatively well-conserved hydrophobic motifs (Fig. 5 b), although there is no clear consensus binding sequence. To validate the interactions, we analyzed the binding to full-length MIND by ITC. Peptide 1 (residues 800–829) bound to the MIND complex in a 1:1 ratio with comparable affinity with NDC80 (Fig. 5 c). Unfortunately, we were unable to purify sufficient quantities of peptide 2, (probably because of the hydrophobic character of the sequence) to obtain a clear binding isotherm. The existence of multiple large binding sites on the Spc105 C terminus suggests that the interactions with MIND are fairly extensive and probably involve multiple members of the complex.

Phosphorylation of the MIND complex by Ipl1p

It has previously been reported that a large number of inner kinetochore proteins, including Dsn1p are directly phosphorylated by the budding yeast Aurora B kinase Ipl1p (Cheeseman et al., 2002; Westermann et al., 2003). We tested this with our recombinant proteins in vitro using Ipl1p and noticed a small

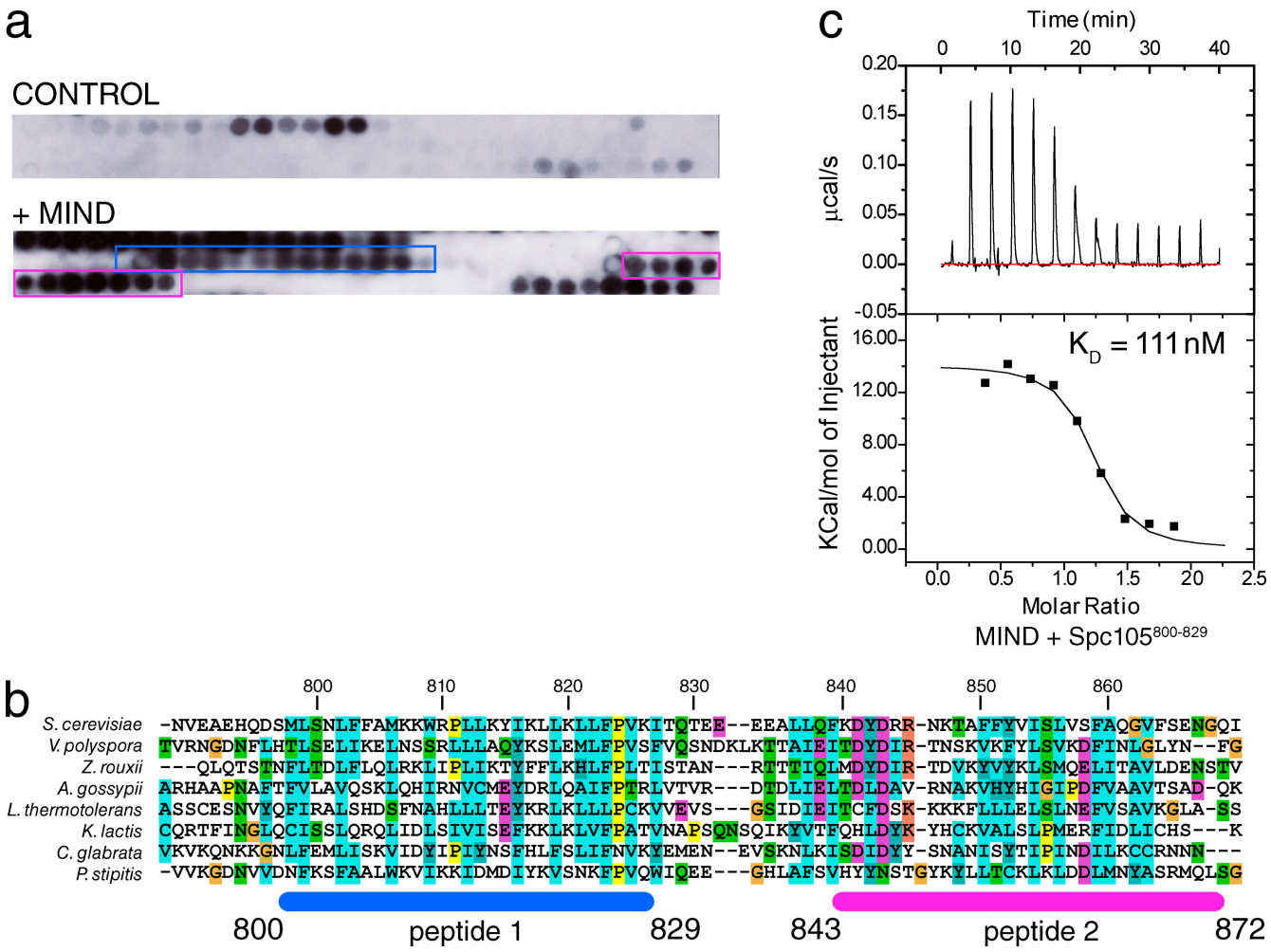

Figure 5. **Characterization of interactions between MIND and Spc105p C terminus.** (a) Peptide array assay for interactions between full-length MIND and Spc105p. The two runs of peptides that exhibit strong interactions are highlighted in blue and pink. (b) Sequence alignment of the C terminus of eight fungal orthologues of Spc105. The sequences corresponding to the peptides that bind MIND are indicated below the alignment in the same color scheme. The colors in the sequences represent different classes of amino acid (turquoise, hydrophobic; purple, acidic; salmon, basic; orange, glycine; yellow, proline; and green, uncharged polar). (c) ITC raw data and binding isotherm for the interaction between MIND and Spc105$^{800–829}$ (peptide 1). The red line is a normalized baseline for the experiment.

but consistent shift in the migration of the Dsn1p band on an SDS-PAGE gel. This shift could be obtained using purified Ipl1p alone; however, the rate and extent of the phosphorylation was greater when using Ipl1p bound to the activating IN-box peptide (Adams et al., 2001). By analyzing the proteins on a PhosTag (Kinoshita et al., 2004) acrylamide gel, the shift of the Dsn1p band was more pronounced (Fig. 6 a). The location of the modification was determined by mass spectrometry (Fig. S1 d). Consistent with a previous study (Westermann et al., 2003), we found that the Dsn1p protein was phosphorylated on Ser250 in an Ipl1p-dependent manner. No other phosphorylation sites in either Dsn1p or any of the other constituents of the MIND complex were found. We tested whether the phosphorylation of Dsn1 affected assembly of either the MIND complex or the interaction with other members of the MKN network. The phosphorylated complex showed normal stoichiometry (not depicted) and bound both NDC80 and the Spc105 C terminus with approximately wild-type affinity (Fig. 6 b). Interestingly, a recent study (Welburn et al., 2010) has shown the Aurora B–mediated phosphorylation of several targets in the human and nematode KMN network, including Dsn1. One of the residues identified as an Aurora B target, Ser109 in human and chicken Dsn1, lies within the same weakly conserved motif as the yeast Ser250, suggesting some similarity in the mechanisms of phosphoregulation between species.

Comparison with the human Mis12 complex

Kinetochore proteins are typically highly divergent at a sequence level, but they are likely to be conserved at the level of three-dimensional structure, and recent crystal structures of the Ndc80 complex from yeast (Wei et al., 2007) and humans (Ciferri et al., 2008) support this hypothesis. Comparison of the *S. cerevisiae* MIND and *Homo sapiens* Mis12 proteins shows a low level of overall sequence identity, at 16%, 23%, 15%, and 14% for Dsn1p, Mtw1p, Nsl1p, and Nnf1p, respectively. However, careful analysis of the sequences and predicted secondary structure motifs led us to suggest that the overall structures are

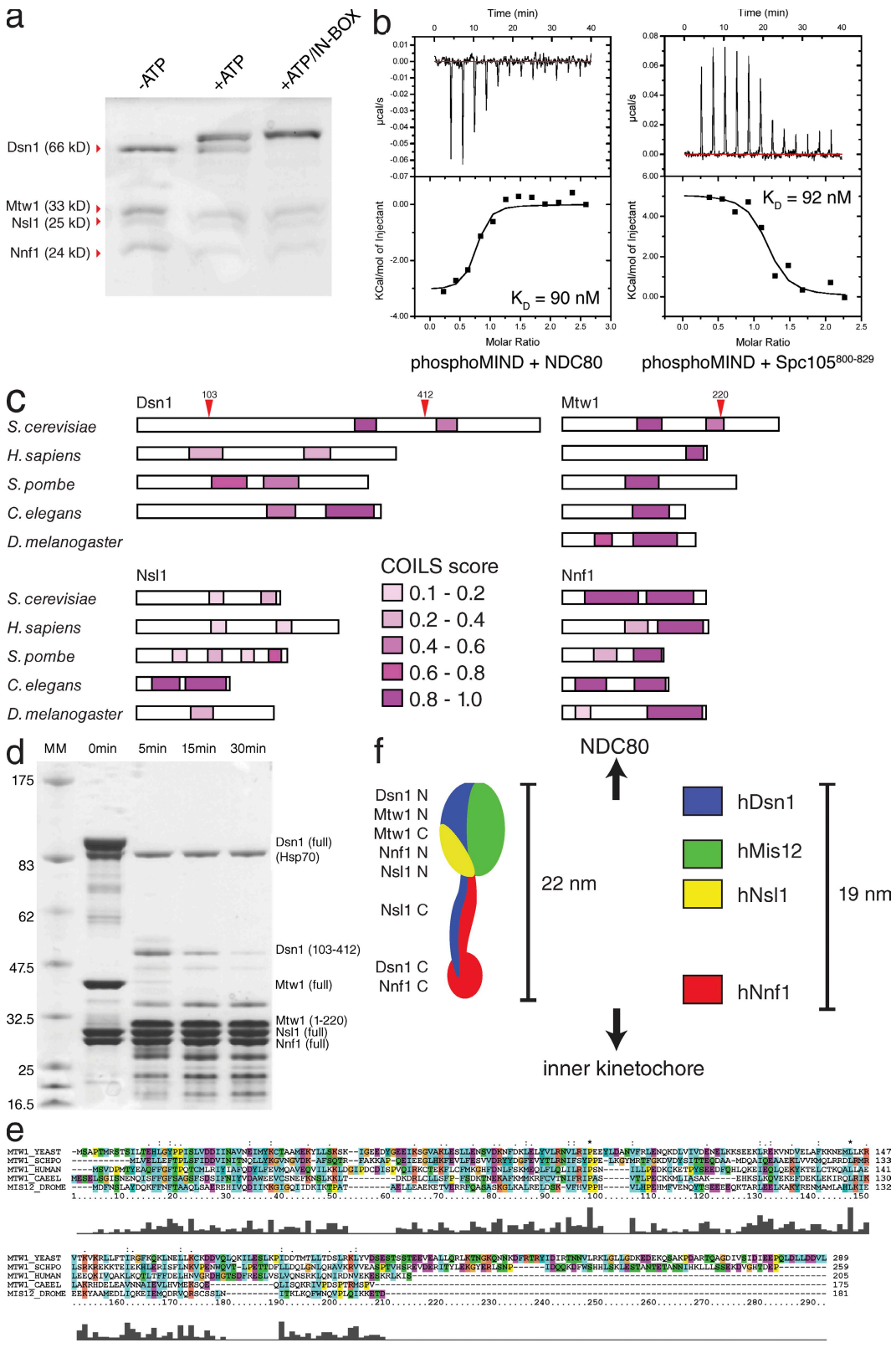

Figure 6. **Phosphorylation of MIND and relationship to the vertebrate Mis12 complex.** (a) Phosphorylation of the MIND complex by the yeast Aurora B homologue, Ipl1, with and without the activating IN-box peptide. (b) ITC raw data and binding isotherms for Ser250 phosphorylated MIND and full-length NDC80 or Spc105$^{800–829}$. The red lines are normalized baselines for the experiment. (c) Comparison of the predicted structural features of five MIND orthologues. The bar length is proportional to the size of the protein. The purple boxes represent predicted coiled-coil segments (assessed using the COILS algorithm; Lupas et al., 1991), with the shading representing the confidence score. The positions of the proteolytic cleavage in the recombinant *S. cerevisiae* proteins are indicated with red arrowheads. (d) Limited proteolysis of the MIND complex using trypsin with the stable truncated products labeled. Molecular mass (MM) is indicated in kilodaltons. (e) Sequence alignment of five Mis12/Mtw1 orthologues. Both the budding and fission yeast proteins contain an extended C-terminal segment that is susceptible to proteolysis. The colors represent different

likely to be similar, as would be expected given their functional conservation. The budding yeast Dsn1p (65.7 kD) and Mtw1p (33.2 kD) proteins are considerably larger than their human orthologues (40 kD and 24.1 kD, respectively; Fig. 6 c). The difference in size appears to be caused by a series of insertions in Dsn1p and an extended C terminus of Mtw1p relative to the human proteins. Notably, the diverged extended regions in the yeast proteins are predicted to be unstructured and would not substantially alter the overall shape of the proteins. Limited proteolysis of the intact MIND complex shows protease-accessible sites at the boundaries of these extended sections (Fig. 6 d). The truncated complex, comprising residues 103–412 of Dsn1p and 1–220 of Mtw1p, still forms a stable tetramer. The protease-resistant domain of Mtw1p is 25.2 kD in size, which is comparable with human Mis12. Sequence alignments of Mtw1p (Fig. 6 e) show that the yeast protein contains a nonconserved C-terminal extension relative to the human proteins, which is removed by protease, leaving a structurally conserved core. The truncated Dsn1p lacks a nonconserved N-terminal extension but also a conserved segment in the C terminus, which our EM experiments indicate lies in the tail domain. As this complex is still stable, the protease-resistant core (predicted to lie in the head) must contain all the interfaces required for tetramer formation, and so is presumably the main site of oligomerization. Based on our localization experiments of the yeast proteins, we would expect the human complex to have a similar overall shape, but perhaps with less pronounced head and tail domains. Recent EM experiments (see Petrovic et al. in this issue) suggest that this is indeed the case.

Discussion

This work describes the first structural characterization of an essential component of the kinetochore MT attachment site. Biochemical analyses show that MIND and NDC80 bind in a 1:1 ratio and that each complex is a single tetramer. In vivo estimates of kinetochore protein composition by quantitative fluorescence microscopy suggest that there are six to seven MIND complexes and eight NDC80 complexes per metaphase kinetochore (Joglekar et al., 2006). Given the relatively tight binding and stoichiometry of the MIND–NDC80 interaction, we suggest that all NDC80s are bound to MIND in the intact kinetochore. In higher eukaryotes, it is possible that NDC80 might be retained at the kinetochore independently of Mis12 by the CENP-H protein (Okada et al., 2006; Cheeseman et al., 2008), but the equivalent interaction with the yeast CENP-H orthologue, Mcm16p, has not been shown, and it seems unlikely that this is the dominant mode of NDC80 attachment. Although we have been unable to reconstitute the entire KMN network because of difficulties expressing full-length Spc105p–Knl1, our peptide assays show that this protein also directly binds the complex in stoichiometric amounts as has been proposed for the *C. elegans* KMN network. (Cheeseman et al., 2006). We have not been able to definitively identify which sections of MIND bind to NDC80 and Spc105p. An accompanying paper (Petrovic et al., 2010) shows that the interaction between the human Mis12 complex and Knl1 is mediated by the C terminus of Nsl1, which is only conserved in vertebrates. Given the considerable variation between Knl1 and Spc105p, it seems reasonable to assume that the mode of binding might be quite different in yeast. This is supported by sequence analysis and results presented in this study, which show a far more hydrophobic interaction between MIND and the Spc105p C terminus compared with the predominantly ionic interaction seen with the human proteins.

The results of our phosphorylation experiments show that although Dsn1p is readily phosphorylated by Ipl1p at a single site, this modification does not significantly affect either the assembly of the MIND complex or the interactions between MIND, NDC80, and Spc105p. Phosphomimetic, or phosphorylation-incompetent mutations of Dsn1p Ser250 do not appear to have any affect on yeast viability (Westermann et al., 2003), and recent work on the Mis12 complex in higher eukaryotes demonstrates that Aurora B activity does not directly affect the assembly or recruitment of the KMN network (Welburn et al., 2010). However, this phosphorylation occurs in a tension-dependent manner, and differential phosphorylation of the target proteins does affect overall MT attachment. This has been proposed to allow fine-tuning of the kinetochore–MT interface, and it will be interesting to see whether such a mechanism is conserved throughout evolution.

The hydrodynamic data and heterogeneity seen in the EM images indicate that the MIND complex is flexible and has considerable structural plasticity. This is similar to the situation seen in NDC80, in which a hinge region in the coiled-coil domain allows the complex to assume differing conformations of currently unknown significance (Wang et al., 2008). Super-resolution light microscopy of the yeast (Joglekar et al., 2009) and human (Wan et al., 2009) kinetochores has shown that the MIND–Mis12 complex may adopt different states during the metaphase to anaphase transition or upon taxol addition. The yeast Nsl1p was reported to move inwards (toward chromatin) during late anaphase, suggesting that the complex might adopt stretched or closed conformations depending on intrakinetochore tension. Similarly, the human Mis12 complex shows large rearrangements upon taxol addition and loss of kinetochore tension with a substantial movement of the human Dsn1 protein. It is difficult to precisely correlate these movements with the predicted intracomplex protein locations described in this work, but the relative static positions of the constituent proteins derived from light microscopy are entirely consistent with the structural data presented here (Fig. 6 f), allowing for uncertainty in the location of the immunofluorescence epitopes. The width of the head (8 nm), as calculated from both EM and SAXS data, and the open, hook shape it adopts strongly suggest that multiple proteins or protein domains form

classes of amino acid (turquoise, hydrophobic; purple, acidic; salmon, basic; orange, glycine; yellow, proline; and green, uncharged polar). (f) Model of the MIND complex showing predicted locations of the proteins based on the data presented in this work (left) and in vivo locations of the human Mis12 proteins derived from light microscopy (right).

a U shape around a central channel. It is tempting to suggest that this may undergo substantial rearrangements or unfolding when under tension, which results in the movements observed by microscopy. This could modulate access of other proteins, for example in the spindle checkpoint, to the appropriate binding sites in MIND.

It is clear from both biochemical experiments and EM images that the interaction between MIND and NDC80 occurs through the Spc24p–Spc25p globular domains and the globular head of MIND. Although we cannot pinpoint the NDC80-binding site on MIND, our EM experiments suggest that it lies in the head region, involving the Dsn1 N terminus, Mtw1, and Nsl1. This then suggests that the tail domain makes contacts with the inner kinetochore proteins, specifically through the Dsn1p and Nnf1p C termini. Although interactions between MIND and inner kinetochore proteins have been reported (De Wulf et al., 2003; Westermann et al., 2003), it is not clear which protein within the complex is involved in mediating the binding. Further biochemical and structural work will undoubtedly address these issues and provide further insight into the formation and regulation of the kinetochore–MT interface.

Materials and methods

Cloning and expression

The recombinant *S. cerevisiae* MIND complex was expressed in *E. coli*. The *DSN1* gene was cloned into pET28a vector (EMD) using the forward and reverse restriction sites NdeI and XhoI, which code an in-frame N-terminal His tag. MTW1 was cloned into pET22a also using the NdeI and XhoI sites. NNF1 and NSL1 were cloned into the pCDFDuet-1 using sites NcoI–NotI for NNF1 and NdeI–XhoI for NSL1. All three plasmids were transformed into BL21(DE3) RIL cells. Cells were grown at 37°C in Luria broth medium containing 25 mg/liter kanamycin, 50 mg/liter ampicillin, and 100 mg/liter spectinomycin. At an optical density of A_{600} = 0.6, the temperature was reduced to 18°C, and cells were induced using 0.5 mM IPTG and grown for a further 16 h. Cells were harvested by centrifugation at 4,000 *g*, and the pellet was resuspended in 50 mM Tris, pH 7.5, 500 mM NaCl, 9% (vol/vol) glycerol, and 0.5% Tween 20, with 1 protease inhibitor cocktail tablet (Roche) for every 40 ml of suspension. The recombinant *S. cerevisiae* NDC80 complex was also expressed in *E. coli*. NUF2 and SPC25 were cloned into pRSFduet vector (EMD) using sites NcoI–EcoRI for NUF2 and NdeI–XhoI for SPC25. NDC80 and SPC24 were cloned into pETduet (EMD) using sites BamHI–NotI for NDC80 coding for an in-frame N-terminal His tag and NdeI–XhoI sites for SPC24. Both plasmids were transformed into BL21(DE3) RIL cells. Cells were grown, and protein was expressed in the same manner as the MIND complex. For production of the Spc24p–Spc25p dimer, SPC24 was cloned into pET22 vector using sites NdeI–EcoRI, and SPC25 was cloned into pET28 vector using sites NdeI–XhoI coding for an in-frame N-terminal His tag. The globular domains of Spc24p–Spc25p were made by cloning SPC24 residues 154–213 and SPC25 residues 133–221 into pRSFduet vector using sites BamHI–NotI for SPC24 154–213 and NdeI–XhoI for SPC25 133–221. Cell growth and expression were performed as described for the MIND complex.

Purification

Cells were lysed by sonication on ice using seven 30-s pulses, and cell debris was pelleted by centrifugation at 18,500 *g* for 1 h at 4°C. The supernatant was passed through a 0.22-µm filter and loaded onto a 5-ml HisTrap FF column (GE Healthcare) preequilibrated in Ni-loading buffer (50 mM Tris, pH 7.5, 500 mM NaCl, 5 mM β-mercaptoethanol, and 2 mM imidazole), followed by elution with a 2–500-mM imidazole gradient over 10 column volumes (c.v.). The fractions containing the MIND complex were further purified by size-exclusion chromatography using a Superdex 200 16/60 (GE Healthcare) equilibrated in gel filtration buffer (50 mM Tris, pH 8.5, 100 mM NaCl, and 5 mM β-mercaptoethanol), followed by ion-exchange chromatography using a Mono Q 5/50 GL column (GE Healthcare) in 50 mM Tris buffer, pH 8.5, and eluted using a 0.1–1-M NaCl gradient over 50 c.v. The Dsn1p–Nsl1p and Mtw1p–Nnf1p heterodimers were made by cloning the respective genes into pET22a and pET28a vectors and coexpressing the two proteins. The dimers were purified in the same manner as the full-length complex. GST and MBP N-terminal fusions were purified as described for the MIND complex, making use of a hexahistidine tag on the N-terminal end of the fusion protein. C-terminal fusion constructs were grown up as per the untagged complex, with the addition of 0.2% (vol/vol) glucose in the medium. Constructs were initially purified by Ni affinity and ion-exchange chromatography as described for the MIND complex, followed by binding to amylose affinity resin (New England Biolabs, Inc.), and eluted with 10 mM maltose in the standard buffer. The protein-containing fractions were pooled and concentrated and run on a Superdex 200 10/300 GL size-exclusion column. This procedure resulted in essentially pure full-length fusion protein. The NDC80 complex was purified in a similar manner to MIND, with the omission of the MonoQ ion-exchange step. The Spc24p–Spc25p dimers and globular domains were purified in the same manner as the full-length NDC80 complex, with the substitution of the S200 gel filtration column by an S75 column.

Negative staining

6 µl of 0.05 mg/ml recombinant MIND complex was deposited onto a freshly glow-discharged, carbon-coated copper grid, blotted after 1 min, and stained with 2% uranyl acetate for 1 min. Specimens were examined in an electron microscope (model 1010; JEOL) operated at 80 kV using a charge-coupled device (Bioscan; Gatan). Images were acquired using DigitalMicrograph (Gatan). Particle picking, classification, and two-dimensional averaging were performed using the EMAN suite of programs (Ludtke et al., 1999). Other measurements were performed using ImageJ (National Institutes of Health). Gold labeling was performed using Ni-NTA-Nanogold (Nanoprobes). NDC80 complex was buffer exchanged into a minimal buffer (30 mM Tris, pH 7.5, and 150 mM NaCl), and then 0.5 nmol of the complex was incubated with 5 nmol of Ni-NTA-Nanogold solution for 30 min at 4°C, followed by gel filtration to eliminate the unbound gold. The 1.8-nm nanogold particle cannot be observed directly under negative-stain conditions. Therefore, we enhanced the particle by placing serial dilutions of nanogold-labeled complex onto carbon-coated grids, blotted residual fluid after 1 min, and then floated the grid on 10 µl of Goldenhance (Nanoprobes) for 30 s. Grids were rinsed in distilled water, stained with 2% uranyl acetate for 1 min, and visualized as described for the unlabeled MIND complex.

Low-angle rotary shadowing

Purified MIND complex at 0.2 mg/ml was mixed with 155 mM ammonium acetate, pH 7.0, and glycerol in a 1:1:3 ratio. 20 µl of the mixture was sprayed onto a freshly cleaved mica surface and dried under vacuum for 1 h at room temperature. Specimens were rotary shadowed with a layer of 2-nm platinum/carbon at an angle of 7.5°, followed by a layer of 10-nm carbon at an angle of 90°. The replicas were floated off onto distilled water and picked up with 400-mesh copper grids. The specimens were examined in a JEOL 1010 electron microscope operated at 80 kV.

AUC

Protein was concentrated to between 0.1 and 0.5 mg/ml in a buffer containing 50 mM Tris, pH 7.5, and 100 mM NaCl. Samples were spun at 40,000 rpm for 24 h at 16°C in an An-50 Ti rotor (Beckman Coulter). Data were analyzed using the program SEDFIT (Schuck, 2000) assuming a continuous c(s) distribution with no prior knowledge. The buffer density was calculated as 1.0089 g/cm^3, and the partial specific volume of the protein was calculated as 0.733 cm^3/g.

SAXS

Proteins were analyzed at concentrations between 0.1 and 1.0 mg/ml in a buffer containing 50 mM Tris, pH 7.5, 100 mM NaCl, and 2 mM dithiothreitol. Data were collected on beamline X33 at the European Molecular Biology Laboratory Hamburg DESY (Deutsches Elektronen-Synchrotron) synchrotron.

All data manipulations were performed using the ATSAS 2.1 suite of programs (European Molecular Biology Laboratory Hamburg). Scattering curves were background-subtracted and analyzed using the program PRIMUS. Individual curves were checked for the presence of aggregation and fitted using the Guinier approximation for the appropriate range, giving a radius of gyration (R_G) of 7.17 ± 0.43 nm. The best curves were scaled and merged, and the final composite curve was transformed into a real-space distance distribution using the program GNOM. Estimates for the value of R_{max} were obtained by measurements on EM images. The real space radius of gyration R_G was calculated as 7.1 nm, which is consistent with the reciprocal space value. Bead-type models of the protein were built

using the program DAMMIN. Typically, 30 separate runs were performed on the same initial data, and models were filtered and averaged using DAMAVER. Models were displayed using the program PyMOL (http://www.pymol.org).

Interaction experiments

Purified NDC80 complex was bound to Ni Sepharose 6 Fast Flow resin (GE Healthcare). 50 c.v. of wash buffer (50 mM Tris-HCl, pH 7.5, 100 mM NaCl, and 20 mM imidazole) was passed over the resin, and binding was confirmed by analysis of the resin using SDS-PAGE. The His tag on the DSN1 subunit of the MIND complex was removed by the addition of tobacco etch virus (TEV) protease (at a ratio of 1:50 TEV to MIND) at 4°C overnight. Undigested MIND complex still containing the His tag and TEV (including a noncleavable His tag) was removed by passing through Ni Sepharose 6 Fast Flow resin. The MIND complex was then added to the resin-bound NDC80 at a molar ratio of 1:1 at 4°C overnight. 50 c.v. of wash buffer was flowed through the column, and then the interacting complex was eluted using wash buffer containing 250 mM imidazole and analyzed using SDS-PAGE. A similar procedure was also performed for the His-tagged SPC24–SPC25 dimers and His-tagged SPC24–SPC25 globular domains.

ITC

ITC experiments were performed at 30°C using an iTC_{200} (MicroCal). Samples were concentrated in a 50 mM Tris, pH 7.5, 100 mM NaCl, 4% glycerol, and 0.5 mM tris(2-carboxyethyl)phosphine buffer. Protein concentrations were determined using a spectrophotometer (NanoDrop ND-1000; Thermo Fisher Scientific). The concentration of NDC80 in the ITC cell was 4 µM; the concentration of MIND in the injection syringe was 62 µM. 3-µl injections were performed at 1,000 rpm stirring speed with an injection spacing of 3 min. The lyophilized peptides of Spc105p were dissolved in the ITC buffer to a concentration of 100 µM. MIND was concentrated to 7 µM. Experiments were performed at 16°C as described for the MIND–NDC80 interactions. The thermodynamic data were processed with the ORIGIN program (MicroCal).

Peptide array assay

Peptides were synthesized and spotted onto a cellulose membrane. The membrane was activated by washing in 50% ethanol + 10% glacial acetic acid for 1 h and then washed in 20 mM Tris, pH 7.5, 100 mM NaCl, and 250 µM tris(2-carboxyethyl)phosphine. 0.6 µg/ml of His-tagged MIND complex was added to the solution along with 0.1% Tween 20 and 0.5% milk and left to incubate at 4°C overnight. The membrane was then incubated with anti-His mouse monoclonal IgG1 antibody for 4 h at room temperature. After further washes, spots with bound MIND complex were detected using rabbit anti–mouse IgG-HRP–conjugated secondary antibody and visualized by chemiluminescence.

Phosphorylation assay

The MIND complex was incubated in a phosphorylation buffer consisting of 50 mM Tris, pH 7.5, 150 mM NaCl, 10 mM $MgCl_2$, and 5 mM ATP. Recombinant *S. cerevisiae* Ipl1 (Aurora B) kinase was added at a molar ratio of 1:100 (Ipl1/MIND complex). The reaction was incubated for 3 h at room temperature. The phosphorylation was analyzed by SDS-PAGE. A 10% separating gel was used containing 50 µM PhosTag ligand and 50 µM $MnCl_2$. The gel was run at 170 V for 1 h and stained using Coomassie brilliant blue. All bands were excised, and phosphorylation sites were mapped by MALDI-TOF (matrix-assisted laser desorption/ionization–time of flight) mass spectrometry.

Limited proteolysis

Trypsin (Sigma-Aldrich) was added in a 1:150 molar ratio to the MIND complex in a buffer consisting of 50 mM Tris, pH 7.5, and 150 mM NaCl. Aliquots were taken at various time points, and proteolysis was stopped by adding SDS loading buffer and heating for 10 min at 100°C. Protein fragments were separated using SDS-PAGE and stained using Coomassie brilliant blue. A separate gel was washed in 50 mM Tris, pH 8.5, and 10% methanol, transferred onto a polyvinylidene fluoride transfer membrane (GE Healthcare), and stained using a membrane stain (40% [vol/vol] methanol, 1% [vol/vol] acetic acid, and 0.1% [vol/vol] Coomassie brilliant blue). The membrane was dried, and the bands were analyzed by Edman sequencing (University of Aberdeen mass spectrometry service).

Online supplemental material

Fig. S1 shows supporting EM images, SAXS reconstructions, and raw mass spectrometry data. Online supplemental material is available at http://www.jcb.org/cgi/content/full/jcb.201002059/DC1.

We wish to thank A. Musacchio for communicating results before publication and F. Uhlmann for helpful comments on the manuscript. We also wish to thank C. Gorba for assistance with SAXS data collection, H. Armer for assistance with EM, and P. Knowles for advice on ITC experiments. N. Michael carried out mass spectrometry in the London Research Institute Protein Analysis facility, and the Peptide Synthesis unit prepared the peptide arrays. SAXS data were collected on beamline X33 of the European Molecular Biology Laboratory DESY synchrotron facility.

This work was funded by Cancer Research UK.

Submitted: 11 February 2010
Accepted: 9 August 2010

References

Adams, R.R., D.M. Eckley, P. Vagnarelli, S.P. Wheatley, D.L. Gerloff, A.M. Mackay, P.A. Svingen, S.H. Kaufmann, and W.C. Earnshaw. 2001. Human INCENP colocalizes with the Aurora-B/AIRK2 kinase on chromosomes and is overexpressed in tumour cells. *Chromosoma*. 110:65–74. doi:10.1007/s004120100130

Cheeseman, I.M., S. Anderson, M. Jwa, E.M. Green, J. Kang, J.R. Yates III, C.S. Chan, D.G. Drubin, and G. Barnes. 2002. Phospho-regulation of kinetochore-microtubule attachments by the Aurora kinase Ipl1p. *Cell*. 111:163–172. doi:10.1016/S0092-8674(02)00973-X

Cheeseman, I.M., S. Niessen, S. Anderson, F. Hyndman, J.R. Yates III, K. Oegema, and A. Desai. 2004. A conserved protein network controls assembly of the outer kinetochore and its ability to sustain tension. *Genes Dev.* 18:2255–2268. doi:10.1101/gad.1234104

Cheeseman, I.M., J.S. Chappie, E.M. Wilson-Kubalek, and A. Desai. 2006. The conserved KMN network constitutes the core microtubule-binding site of the kinetochore. *Cell*. 127:983–997. doi:10.1016/j.cell.2006.09.039

Cheeseman, I.M., T. Hori, T. Fukagawa, and A. Desai. 2008. KNL1 and the CENP-H/I/K complex coordinately direct kinetochore assembly in vertebrates. *Mol. Biol. Cell*. 19:587–594. doi:10.1091/mbc.E07-10-1051

Ciferri, C., J. De Luca, S. Monzani, K.J. Ferrari, D. Ristic, C. Wyman, H. Stark, J. Kilmartin, E.D. Salmon, and A. Musacchio. 2005. Architecture of the human ndc80-hec1 complex, a critical constituent of the outer kinetochore. *J. Biol. Chem.* 280:29088–29095. doi:10.1074/jbc.M504070200

Ciferri, C., S. Pasqualato, E. Screpanti, G. Varetti, S. Santaguida, G. Dos Reis, A. Maiolica, J. Polka, J.G. De Luca, P. De Wulf, et al. 2008. Implications for kinetochore-microtubule attachment from the structure of an engineered Ndc80 complex. *Cell*. 133:427–439. doi:10.1016/j.cell.2008.03.020

De Wulf, P., A.D. McAinsh, and P.K. Sorger. 2003. Hierarchical assembly of the budding yeast kinetochore from multiple subcomplexes. *Genes Dev.* 17:2902–2921. doi:10.1101/gad.1144403

DeLuca, J.G., Y. Dong, P. Hergert, J. Strauss, J.M. Hickey, E.D. Salmon, and B.F. McEwen. 2005. Hec1 and nuf2 are core components of the kinetochore outer plate essential for organizing microtubule attachment sites. *Mol. Biol. Cell*. 16:519–531. doi:10.1091/mbc.E04-09-0852

Euskirchen, G.M. 2002. Nnf1p, Dsn1p, Mtw1p, and Nsl1p: a new group of proteins important for chromosome segregation in *Saccharomyces cerevisiae*. *Eukaryot. Cell*. 1:229–240. doi:10.1128/EC.1.2.229-240.2002

Goshima, G., and M. Yanagida. 2000. Establishing biorientation occurs with precocious separation of the sister kinetochores, but not the arms, in the early spindle of budding yeast. *Cell*. 100:619–633. doi:10.1016/S0092-8674(00)80699-6

Goshima, G., S. Saitoh, and M. Yanagida. 1999. Proper metaphase spindle length is determined by centromere proteins Mis12 and Mis6 required for faithful chromosome segregation. *Genes Dev.* 13:1664–1677. doi:10.1101/gad.13.13.1664

Joglekar, A.P., D.C. Bouck, J.N. Molk, K.S. Bloom, and E.D. Salmon. 2006. Molecular architecture of a kinetochore-microtubule attachment site. *Nat. Cell Biol.* 8:581–585. doi:10.1038/ncb1414

Joglekar, A.P., K. Bloom, and E.D. Salmon. 2009. In vivo protein architecture of the eukaryotic kinetochore with nanometer scale accuracy. *Curr. Biol.* 19:694–699. doi:10.1016/j.cub.2009.02.056

Kinoshita, E., M. Takahashi, H. Takeda, M. Shiro, and T. Koike. 2004. Recognition of phosphate monoester dianion by an alkoxide-bridged dinuclear zinc(II) complex. *Dalton Trans.* (8):1189–1193. doi:10.1039/b400269e

Kiyomitsu, T., C. Obuse, and M. Yanagida. 2007. Human Blinkin/AF15q14 is required for chromosome alignment and the mitotic checkpoint through direct interaction with Bub1 and BubR1. *Dev. Cell*. 13:663–676. doi:10.1016/j.devcel.2007.09.005

Kline, S.L., I.M. Cheeseman, T. Hori, T. Fukagawa, and A. Desai. 2006. The human Mis12 complex is required for kinetochore assembly and proper chromosome segregation. *J. Cell Biol.* 173:9–17. doi:10.1083/jcb.200509158

Ludtke, S.J., P.R. Baldwin, and W. Chiu. 1999. EMAN: semiautomated software for high-resolution single-particle reconstructions. *J. Struct. Biol.* 128:82–97. doi:10.1006/jsbi.1999.4174

Lupas, A., M. Van Dyke, and J. Stock. 1991. Predicting coiled coils from protein sequences. *Science*. 252:1162–1164. doi:10.1126/science.252.5009.1162

McAinsh, A.D., P. Meraldi, V.M. Draviam, A. Toso, and P.K. Sorger. 2006. The human kinetochore proteins Nnf1R and Mcm21R are required for accurate chromosome segregation. *EMBO J.* 25:4033–4049. doi:10.1038/sj.emboj.7601293

Meraldi, P., A.D. McAinsh, E. Rheinbay, and P.K. Sorger. 2006. Phylogenetic and structural analysis of centromeric DNA and kinetochore proteins. *Genome Biol.* 7:R23. doi:10.1186/gb-2006-7-3-r23

Musacchio, A., and E.D. Salmon. 2007. The spindle-assembly checkpoint in space and time. *Nat. Rev. Mol. Cell Biol.* 8:379–393. doi:10.1038/nrm2163

Okada, M., I.M. Cheeseman, T. Hori, K. Okawa, I.X. McLeod, J.R. Yates III, A. Desai, and T. Fukagawa. 2006. The CENP-H-I complex is required for the efficient incorporation of newly synthesized CENP-A into centromeres. *Nat. Cell Biol.* 8:446–457. doi:10.1038/ncb1396

Petrovic, A., S. Pasqualato, P. Dube, V. Krenn, S. Santaguida, D. Cittaro, S. Monzani, L. Massimiliano, J. Keller, A. Tarricone, A. Maiolica, H. Stark, and A. Musacchio. 2010. The MIS12 complex is a protein interaction hub for outer kinetochore assembly. *J. Cell Biol.* 190:835–852. doi:10.1083/jcb.201002070.

Przewloka, M.R., W. Zhang, P. Costa, V. Archambault, P.P. D'Avino, K.S. Lilley, E.D. Laue, A.D. McAinsh, and D.M. Glover. 2007. Molecular analysis of core kinetochore composition and assembly in *Drosophila melanogaster*. *PLoS One*. 2:e478. doi:10.1371/journal.pone.0000478

Santaguida, S., and A. Musacchio. 2009. The life and miracles of kinetochores. *EMBO J.* 28:2511–2531. doi:10.1038/emboj.2009.173

Scharfenberger, M., J. Ortiz, N. Grau, C. Janke, E. Schiebel, and J. Lechner. 2003. Nsl1p is essential for the establishment of bipolarity and the localization of the Dam-Duo complex. *EMBO J.* 22:6584–6597. doi:10.1093/emboj/cdg636

Schuck, P. 2000. Size-distribution analysis of macromolecules by sedimentation velocity ultracentrifugation and lamm equation modeling. *Biophys. J.* 78:1606–1619. doi:10.1016/S0006-3495(00)76713-0

Shan, X., Z. Xue, G. Euskirchen, and T. Mélèse. 1997. NNF1 is an essential yeast gene required for proper spindle orientation, nucleolar and nuclear envelope structure and mRNA export. *J. Cell Sci.* 110:1615–1624.

Wan, X., R.P. O'Quinn, H.L. Pierce, A.P. Joglekar, W.E. Gall, J.G. DeLuca, C.W. Carroll, S.-T. Liu, T.J. Yen, B.F. McEwen, et al. 2009. Protein architecture of the human kinetochore microtubule attachment site. *Cell*. 137:672–684. doi:10.1016/j.cell.2009.03.035

Wang, H.W., S. Long, C. Ciferri, S. Westermann, D. Drubin, G. Barnes, and E. Nogales. 2008. Architecture and flexibility of the yeast Ndc80 kinetochore complex. *J. Mol. Biol.* 383:894–903. doi:10.1016/j.jmb.2008.08.077

Wei, R.R., P.K. Sorger, and S.C. Harrison. 2005. Molecular organization of the Ndc80 complex, an essential kinetochore component. *Proc. Natl. Acad. Sci. USA*. 102:5363–5367. doi:10.1073/pnas.0501168102

Wei, R.R., J. Al-Bassam, and S.C. Harrison. 2007. The Ndc80/HEC1 complex is a contact point for kinetochore-microtubule attachment. *Nat. Struct. Mol. Biol.* 14:54–59. doi:10.1038/nsmb1186

Welburn, J.P.I., M. Vleugel, D. Liu, J.R. Yates III, M.A. Lampson, T. Fukagawa, and I.M. Cheeseman. 2010. Aurora B phosphorylates spatially distinct targets to differentially regulate the kinetochore-microtubule interface. *Mol. Cell*. 38:383–392. doi:10.1016/j.molcel.2010.02.034

Westermann, S., I.M. Cheeseman, S. Anderson, J.R. Yates III, D.G. Drubin, and G. Barnes. 2003. Architecture of the budding yeast kinetochore reveals a conserved molecular core. *J. Cell Biol.* 163:215–222. doi:10.1083/jcb.200305100